



## 4-Amino-6-arylaminopyrimidine-5-carbaldehyde hydrazones as potent ErbB-2/EGFR dual kinase inhibitors

Guozhang Xu\*, Marta C. Abad, Peter J. Connolly, Michael P. Neeper, Geoffrey T. Struble, Barry A. Springer, Stuart L. Emanuel, Niranjana Pandey, Robert H. Gruninger, Mary Adams, Sandra Moreno-Mazza, Angel R. Fuentes-Pesquera, Steven A. Middleton

Johnson & Johnson Pharmaceutical Research and Development, Medicinal Chemistry, 8 Clarke Drive, Cranbury, NJ 08512, USA

### ARTICLE INFO

#### Article history:

Received 24 April 2008

Revised 7 July 2008

Accepted 8 July 2008

Available online 10 July 2008

#### Keywords:

Receptor tyrosine kinase

ErbB-2

EGFR

Hydrazones

Quinazoline

Bioisostere

### ABSTRACT

Members of a novel class of 4-amino-6-arylaminopyrimidine-5-carbaldehyde hydrazones were identified as potent dual ErbB-2/EGFR kinase inhibitors using concept-guided design approach. These compounds inhibited the growth of ErbB-2 over-expressing human tumor cell lines (BT474, N87, and SK-BR-3) in vitro. Compound **15** emerged as a key lead and showed significant ability to inhibit growth factor-induced receptor phosphorylation in SK-BR-3 cells ( $IC_{50}$  = 54 nM) and cellular proliferation in vitro ( $IC_{50}$  = 14, 58, and 58 nM for BT474, N87, and SK-BR-3 respectively). The X-ray co-crystal structure of EGFR with a close analog (**17**) was determined and validated our design rationale.

© 2008 Elsevier Ltd. All rights reserved.

The type I receptor tyrosine kinases (RTK) are involved in various aspects of cell growth, survival, and differentiation.<sup>1</sup> Among the known RTKs, the epidermal growth factor receptor (EGFR) and ErbB-2 (HER-2) are two widely studied proteins that are prototypic members of the ErbB family that also includes ErbB-3 (Her-3) and ErbB-4 (HER-4).<sup>2</sup> Over-expression of ErbB-2 and EGFR has been associated with aggressive disease and poor patient prognosis in a range of human tumor types (e.g. breast, lung, ovarian, prostate, and squamous carcinoma of head and neck).<sup>3</sup> Disruption of signal transduction of these kinases has been shown to have an antiproliferative and therapeutic effect.<sup>4</sup> Various approaches have been developed to target the ErbB signaling pathways including monoclonal antibodies (trastuzumab/Herceptin<sup>®</sup> and cetuximab/Erbitux<sup>®</sup>) directed against the receptor and synthetic tyrosine kinase inhibitors (gefitinib/Iressa<sup>®</sup>, **2**, and erlotinib/Tarceva<sup>®</sup>, **4**).<sup>5</sup> Since many tumors over-express ErbB receptors and/or ligands, simultaneous targeting of multiple erbB receptors therefore becomes a promising approach to cancer treatment. Lapatinib (Tykerb<sup>®</sup>, **3**), a potent dual EGFR/ErbB-2 inhibitor, was recently approved for the treatment of ErbB-2 positive breast cancer.<sup>6</sup>

Among various scaffolds employed as ErbB-2/EGFR kinase inhibitors (Fig. 1),<sup>5c,6,7</sup> the 4-anilinoquinazoline scaffold (**2**, **3**, and **4**) is the most commonly utilized template for inhibition of the

ErbB family. The quinazoline moiety fits into the ATP-binding pocket in the kinase domain, while the aniline ring fills an adjacent lipophilic pocket.

In an effort to develop non-anilinoquinazoline small molecular ATP-competitive ErbB-2/EGFR inhibitors as cancer therapeutics, we recently reported a novel series of 4-aminopyrimidine-5-carbaldehyde oximes (**6**)<sup>8</sup> that are potent dual inhibitors of EGFR and ErbB-2 tyrosine kinases (Fig. 2). This scaffold effectively mimics the well-known quinazoline kinase template by forming a pseudo-bicyclic structure with the help of an intramolecular hydrogen bond between the 4-amino group and the oxime nitrogen atom. Further bioisosteric replacement of the oxime moiety with hydrazone leads to aminopyrimidine hydrazone (**7**), in which the intramolecular NH...N=C hydrogen bond is maintained and would function as mimics of the phenyl ring of the quinazoline (Fig. 2). Although the hydrazone side chain is expected to orient toward the solvent front (vide infra), a cyclic *N,N*-disubstituted hydrazone might gain additional kinase potency due to the restricted bond rotation of the side chain. We report here the synthesis and structure–activity relationships (SAR) of this series as dual ErbB-2/EGFR kinase inhibitors and the X-ray crystal structure of representative compound **17** in complex with EGFR.

4-Amino-6-arylaminopyrimidine-5-carbaldehyde hydrazones were synthesized according to the two-step sequence outlined in Scheme 1. Treatment of 4-amino-6-chloro-pyrimidine-5-carbaldehyde (**8**)<sup>9</sup> with the appropriate aniline in DMSO at 100 °C for 3 h

\* Corresponding author. Tel.: +1 609 655 6915; fax: +1 609 655 6930.

E-mail address: [gxu4@prdu.s.jnj.com](mailto:gxu4@prdu.s.jnj.com) (G. Xu).

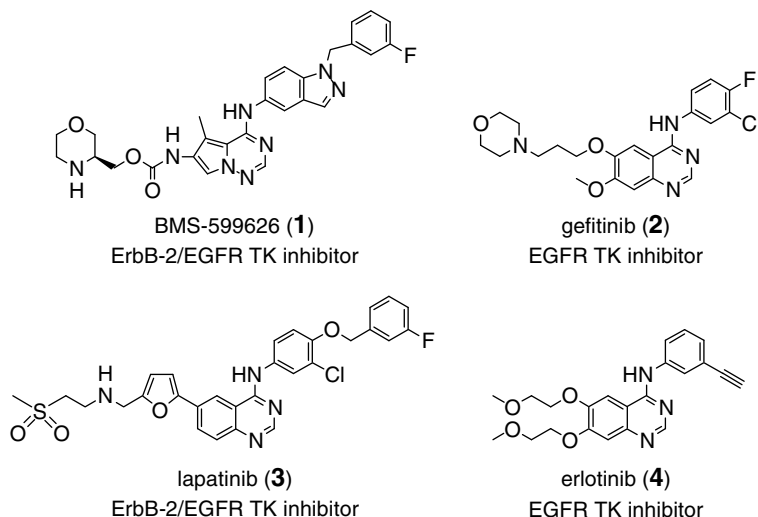


**Figure 1.** Examples of ErbB family TK inhibitors currently approved or in clinical trials for anti-cancer therapy.

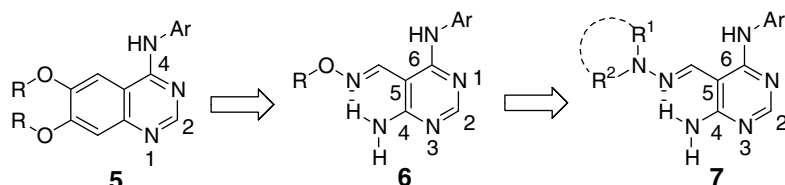
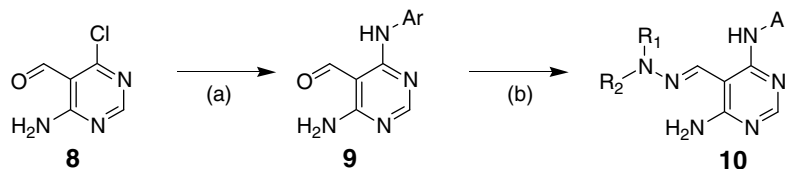


**Figure 2.** Quinazoline (**5**), 4-amino-6-arylaminopyrimidine-5-carbaldehyde oxime (**6**),<sup>8</sup> and hydrazone (**7**) templates.



**Scheme 1.** Reagents and conditions: (a) ArNH<sub>2</sub>, DIPEA, DMSO; (b) R<sup>2</sup>R<sup>1</sup>NHNH<sub>2</sub>, MeOH.

provided the 4-amino-6-arylaminopyrimidine-5-carbaldehyde (**9**). Condensation of (**9**) with various hydrazines in MeOH afforded the aminopyrimidine hydrazones (**10**). In all cases the *E*-isomer was either the major or exclusive product obtained.

In the quinazoline and pyrrolo[2,1-*f*][1,2,4]triazine series,<sup>10,11</sup> it has been demonstrated that larger aniline substitutions confer greater dual ErbB-2 and EGFR tyrosine kinase inhibition. A similar SAR trend was also seen in our 4-aminopyrimidine 5-carbaldehyde oxime scaffold, where increasing size at the C-6 aniline position substantially improved ErbB-2 potency.<sup>8</sup> In pursuit of our goal to improve dual ErbB-2/EGFR activities in the 4-aminopyrimidine hydrazone series, we selected 1-(3-fluorobenzyl)-indazol-5-amino at the C-6 position for our SAR study. Our initial effort focused on the primary hydrazones and Table 1 summarizes the inhibitory activities of these compounds against ErbB-2/EGFR kinases and ErbB-2 receptor phosphorylation in SK-BR-3 cells.<sup>12,13</sup>

In terms of ErbB-2 kinase activity, the primary hydrazone **12** is 7-fold less potent than the corresponding methyl oxime **11**. However, both compounds significantly inhibit ErbB-2 receptor phosphorylation in SK-BR-3 cells. The aryl-substituted primary

**Table 1**

Inhibitory activity of oxime and primary hydrazones–SAR at the C-5 position

Compound	R	ErbB-2 IC <sub>50</sub> <sup>a</sup> (μM)	EGFR IC <sub>50</sub> <sup>a</sup> (μM)	ErbB-2 phosphorylation IC <sub>50</sub> <sup>a</sup> (μM)
<b>11</b> <sup>8</sup>	CH <sub>3</sub> O	0.012	0.008	0.301
<b>12</b>	CH <sub>3</sub> NH	0.084	0.012	0.361
<b>13</b>	CF <sub>3</sub> CH <sub>2</sub> NH	0.020	0.052	0.258
<b>14</b>	4-CH <sub>3</sub> O-C <sub>6</sub> H <sub>4</sub>	0.118	0.049	1.291

<sup>a</sup> Mean values of three experiments are used for ErbB-2 and EGFR enzyme assays and ErbB-2 cellular phosphorylation assay. IC<sub>50</sub> values are reported as μM concentrations.

hydrazone **14** is much less potent in both ErbB-2 and EGFR enzyme assays. Trifluoroethylhydrazone **13** maintains decent ErbB-2 kinase potency as well as significant inhibition of ErbB-2 receptor phosphorylation in SK-BR-3 cells but is less potent against EGFR kinase.

We next turned our attention to di-substituted hydrazones, especially the cyclic *N,N*-disubstituted hydrazones. Table 2 summarizes the inhibitory activities of these compounds against ErbB-2/EGFR kinases and ErbB-2 receptor phosphorylation in SK-BR-3 cells. Antiproliferative activity of selected compounds against four cancer cell lines, BT474 (breast tumor), N87 (gastric tumor), SK-BR-3 (breast carcinoma), and HeLa (cervical adenocarcinoma) are also summarized in Table 2.<sup>14</sup>

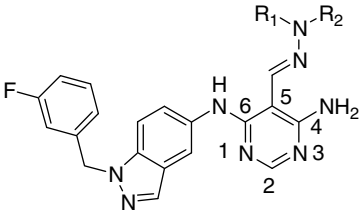
The *N,N*-dimethylhydrazone **15** is 42-fold more potent than *N*-methylhydrazone **12** in the ErbB-2 kinase assay and 3-fold more potent in inhibiting the ErbB-2 receptor phosphorylation. It is also 6-fold more potent than the methyl oxime **11** in the ErbB-2 kinase assay. In the cell antiproliferative assays, *N,N*-dimethylhydrazone **15** significantly inhibits the growth of ErbB-2 over-expressing BT474 (63 nM) and SK-BR-3 (148 nM) cell lines as well as N87 (131 nM) cell line, which over-expresses both ErbB-2 and EGFR. We also tested the oxime **11** in the BT474 and SK-BR-3 antiproliferative assays. It has IC<sub>50</sub> of 254 nM against BT474 cell line and IC<sub>50</sub> of 260 nM against SK-BR-3 cell line. The cyclic *N,N*-disubstituted

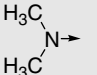
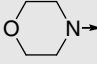
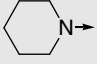
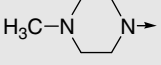
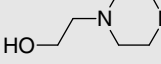
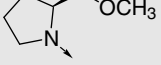
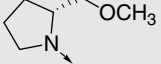
hydrazones **16–21** all remain very potent (IC<sub>50</sub> within the range of 2 to 72 nM) against both ErbB-2 and EGFR kinases. Compounds **16**, **17**, and **19** exhibit very potent antiproliferative activities in BT474, SK-BR-3, and N87 cell lines. All compounds tested do not inhibit the growth of the non-ErbB-2-dependent HeLa cell line (IC<sub>50</sub> > 10 μM), consistent with a cellular mode of action involving inhibition of ErbB-2/EGFR. For reference, lapatinib (**3**) has an IC<sub>50</sub> of 25 nM in the BT474 cell line. The high potency seen for the cyclic *N,N*-disubstituted hydrazones in both enzyme and cell assays is believed to result in part from the restricted bond rotation of the hydrazone side chain, which contributes to good Caco-2 permeability properties of these molecules (data not shown).

To determine kinase selectivity for this series of dual ErbB-2/EGFR inhibitors, analogs **16** and **17** were screened against a panel of 100 kinases at the concentration of 3 μM in the presence of 100 μM ATP.<sup>15</sup> Both compounds were highly selective versus the kinase panel, inhibiting only Lck (71% and 60%, respectively) and c-Raf (47% and 50%, respectively) in addition to EGFR and ErbB-2.

To further validate our design rationale, compound **17** was successfully crystallized with EGFR protein and the X-ray crystal structure of the complex was determined to a resolution of 2.0 Å.<sup>16</sup> The structure reveals that compound **17** binds to the ATP-binding cleft with the amino-pyrimidine ring hydrogen-bonded to the kinase hinge region. Details of the interactions be-

**Table 2**  
Inhibitory activity of *N,N*-disubstituted hydrazones at the C-5 position



Compound	R <sup>2</sup> R <sup>1</sup> N	ErbB-2 IC <sub>50</sub> <sup>a</sup> (μM)	EGFR IC <sub>50</sub> <sup>a</sup> (μM)	ErbB-2 phosphorylation IC <sub>50</sub> <sup>a</sup> (μM)	BT474 <sup>b</sup> (μM)	N87 <sup>c</sup> (μM)	SK-BR-3 <sup>d</sup> (μM)	HeLa <sup>e</sup> (μM)
<b>15</b>		0.002	0.008	0.105	0.063	0.131	0.148	>100
<b>16</b>		0.007	0.016	0.083	0.031	0.091	0.122	>100
<b>17</b>		0.018	0.030	0.148	0.049	0.365	0.691	>10
<b>18</b>		0.008	0.016	0.509	ND <sup>f</sup>	ND <sup>f</sup>	ND <sup>f</sup>	ND <sup>f</sup>
<b>19</b>		0.008	0.009	0.054	0.014	0.058	0.058	>100
<b>20</b>		0.039	0.026	0.426	ND <sup>f</sup>	ND <sup>f</sup>	ND <sup>f</sup>	ND <sup>f</sup>
<b>21</b>		0.072	0.031	ND <sup>f</sup>	ND <sup>f</sup>	ND <sup>f</sup>	ND <sup>f</sup>	ND <sup>f</sup>

<sup>a</sup> Mean values of three experiments are used for ErbB-2 and EGFR enzyme assays and ErbB-2 cellular phosphorylation assay. IC<sub>50</sub> values are reported as micromolar concentrations. IC<sub>50</sub> values listed as >10 or >100 indicate that 50% inhibition was not reached at the highest dose tested (10 or 100 μM, respectively), nor was an inhibition maximum observed.

<sup>b</sup> Breast tumor line over-expressing ErbB-2.

<sup>c</sup> Gastric tumor line over-expressing ErbB-2.

<sup>d</sup> Breast Carcinoma cell line over-expressing ErbB-2.

<sup>e</sup> Cervical adenocarcinoma.

<sup>f</sup> Not determined.

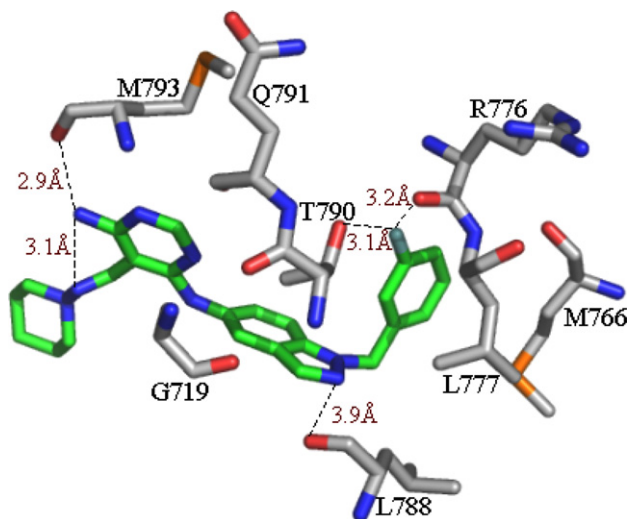


**Figure 3.** Interactions between EGFR and compound **17**. Compound **17** is shown in green, protein residues are colored gray and atoms are colored by element for both molecules with nitrogen blue, oxygen red and fluorine light green.

tween the protein and **17** are shown in Figure 3. The pyrimidine ring nitrogen N3 interacts with the backbone NH of Met793 (not shown), and the amino group at the C-4 position is engaged in a second hydrogen bond with the backbone C=O of Met793. The 1-(3-fluorobenzyl)indazolylamino group is oriented deep in the back of the ATP binding site and makes predominantly hydrophobic interactions with the protein. The 3-fluorobenzyl group occupies a pocket formed by the side chains of Met766, Leu777, Thr790, Thr854 (not shown), and Phe856 (not shown). The 3-fluoro on the benzyl group interacts with both backbone NH groups of Arg776 and Thr790 (3.2 Å and 3.19 Å, respectively). The N-2 atom of the indazole ring forms a weak hydrogen bond to the C=O of Leu788 (3.9 Å).

The aniline nitrogen and the N-1 atom of the indazole ring are not involved in any direct hydrogen-bonding interactions with the protein. The piperidine group of the hydrazone moiety is extended to the solvent-exposed region. The C-4 amino group on the pyrimidine ring clearly forms an intramolecular hydrogen bond with the hydrazone nitrogen atom as we anticipated, therefore mimicking the quinazoline *phenyl* ring.

An overlay of the EGFR-bound conformations of lapatinib (**3**)<sup>17</sup> and compound **17** is shown in Figure 4, which confirms that **17**

binds in a similar fashion to lapatinib (**3**). The overlay between proteins in both crystal structures showed an alignment throughout the protein with a rms deviation value of 0.01096. This comparison also shows a near-perfect alignment between both compounds with the exception of the orientation of the hydrazone moiety in **17** compared to the furan of lapatinib.

Compounds **15**, **16**, and **17** were selected for fast pharmacokinetic evaluation (at four time points: 0.5, 1, 2, and 4 h) in Sprague–Dawley rats, all compounds exhibited very low plasma levels (Table 3). Although most compounds in the series displayed good Caco-2 properties and modest in vitro rat microsomal stability (data not shown), aqueous solubility for most of the 4-amino-pyrimidine hydrazones synthesized was very low, which could account for the poor rat PK profile for **15**, **16**, and **17**. Solubility could be improved by appropriate modification of the R<sup>1</sup> and R<sup>2</sup> substituents on the hydrazone moiety since this region is positioned toward the solvent interface, as shown in the crystal structure of **17** and EGFR.

In summary, 4-amino-6-arylaminopyrimidine-5-carbaldehyde hydrazones have been explored as dual ErbB-2/EGFR kinase inhibitors. The *N,N*-disubstituted hydrazone compounds possess excellent in vitro tyrosine kinase inhibition as well as cellular antiproliferative activity in the ErbB-2 over-expressing BT474, N87 and SK-BR-3 tumor cell lines. One of the optimized compounds, **15**, exhibited IC<sub>50</sub> values of 8 and 9 nM against ErbB-2 and EGFR, respectively, in the kinase assay, and showed potent antiproliferative effect in the ErbB-2 over-expressing tumor cell lines (IC<sub>50</sub> = 14, 58, and 58 nM for BT474, N87, and SK-BR-3 respectively). Consequently, its close analog **17** was co-crystallized in complex with EGFR and the X-ray crystal structure was determined. The X-ray structure showed a nearly identical binding mode as lapatinib (**3**), except that lapatinib makes hinge contact at Met 793,<sup>17</sup> whereas **17** forms a *bidentate* interaction with NH and the carbonyl oxygen of Met793.

**Table 3**

Fast pharmacokinetic evaluation for compounds **15**, **16**, and **17** in Sprague–Dawley rats at 10 mg/kg po

Compound	Concn (ng/mL) at 0.5 h	Concn (ng/mL) at 1 h	Concn (ng/mL) at 2 h	Concn (ng/mL) at 4 h
<b>15</b> <sup>a</sup>	10.1	6.3	13.2	4.6
<b>16</b> <sup>b</sup>	26.1	21.6	1.5	0
<b>17</b> <sup>b</sup>	23.4	12.6	32.4	0

<sup>a</sup> Vehicle = 10% solutol in D5W.

<sup>b</sup> Vehicle = 0.5% hydroxypropyl methylcellulose.

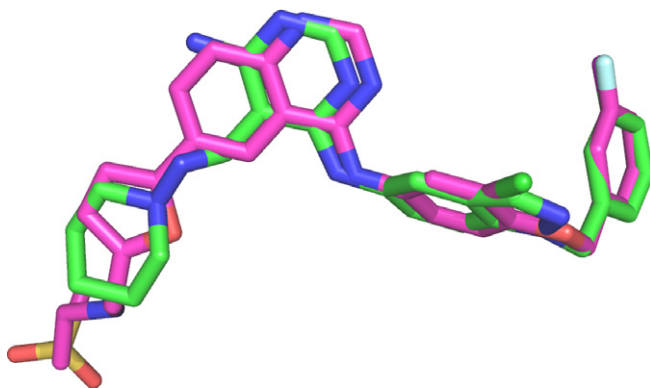


**Figure 4.** Overlay of lapatinib (**3**) onto compound **17**. Compound **17** is shown in green, Lapatinib is colored pink, and atoms are colored by element for both molecules with nitrogen blue, oxygen red, fluorine magenta, chlorine light green, and sulfur yellow.

## Acknowledgments

Use of the IMCA-CAT beamline 17-ID (or 17-BM) at the Advanced Photon Source was supported by the companies of the Industrial Macromolecular Crystallography Association through a contract with the Center for Advanced Radiation Sources at the University of Chicago.

## References and notes

- Olayioye, M. A.; Neve, R. M.; Lane, H. A.; Hynes, N. E. *EMBO J.* **2000**, *19*, 3159.
- (a) Salomon, D. S.; Bradt, R.; Ciardiello, F.; Normanno, N. *Crit. Rev. Oncol. Hematol.* **1995**, *19*, 183; (b) Black, J. D.; Brattain, M. G.; Krishnamurthi, S. A.; Dawson, D. M.; Willson, J. K. *Curr. Opin. Invest. Drugs* **2003**, *4*, 1451.
- (a) Gullick, W. J. *Br. Med. Bull.* **1991**, *47*, 87; (b) Woodburn, J. R. *Pharmacol. Ther.* **1999**, *82*, 241.
- Seymour, L. *Curr. Opin. Invest. Drugs* **2003**, *4*, 658.
- (a) Baselga, J.; Tripathy, D.; Mendelsohn, J.; Baughman, S.; Benz, C. C.; Dantis, L.; Sklarin, N. T.; Seidman, A. D.; Hudis, C. A.; Moore, J.; Rosen, P. P.; Twaddell, T.; Henderson, I. C.; Norton, L. J. *Clin. Oncol.* **1996**, *14*, 737; (b) Waksal, H. W. *Cancer Metastasis Rev.* **2000**, *18*, 427; (c) Gschwind, A.; Fisher, O. M.; Ullrich, A. *Nature* **2004**, 361.
- Rusnak, D. W.; Lackey, K.; Affleck, K.; Wood, E. R.; Alligood, K. J.; Rhodes, N.; Keith, B. R.; Murray, D. M.; Knight, W. B.; Mullin, R. J.; Gilmer, T. M. *Mol. Cancer Ther.* **2001**, *1*, 85.
- (a) Vite, G. D.; Gavai, A. V.; Fink, B. E.; Mastalerz, H.; Kadow, J. F. *PCT Int. Appl. WO2004054514 A2*, 2004; (b) Borman, S. *Chem. Eng. News* **2005**, *83*, 40.
- Xu, G.; Searle, L. L.; Hughes, T. V.; Beck, A. K.; Connolly, P. J.; Abad, M. C.; Neeper, M. P.; Struble, G. T.; Springer, B. A.; Emanuel, S. L.; Gruninger, R. H.; Pandey, N.; Adams, M.; Moreno-Mazza, S.; Fuentes-Pesquera, A. R.; Middleton, S. A.; Greebberger, L. M. *Bioorg. Med. Chem. Lett.* **2008**, *18*, 3495.
- Gomtsyan, A.; Didomenico, S.; Lee, C.; Matulenko, M. A.; Kim, K.; Kowaluk, E. A.; Wismer, C. T.; Mikusa, J.; Yu, H.; Kohlhaas, K.; Jarvis, M. F.; Bhagwat, S. S. *J. Med. Chem.* **2002**, *45*, 3639.
- Gaul, M. D.; Guo, Y.; Affleck, K.; Cockerill, G. S.; Gilmer, T. M.; Griffin, R. J.; Guntrip, S.; Keith, B. R.; Knight, W. B.; Mullin, R. J.; Murray, D. M.; Rusnak, D. W.; Smith, K.; Tadepalli, S.; Wood, E. R.; Lackey, K. *Bioorg. Med. Chem. Lett.* **2003**, *13*, 637.
- Fink, B. E.; Vite, G. D.; Mastalerz, H.; Kadow, J. F.; Kim, S.; Leavitt, K. J.; Du, K.; Crews, D.; Mitt, T.; Wong, T. W.; Hunt, J. T.; Vyas, D. M.; Tokarski, J. S. *Bioorg. Med. Chem. Lett.* **2005**, *15*, 4774.
- The reaction was incubated for 60 min at 30 °C for ErbB-2 (in 60 nM Hepes pH 7.5, 3 mM magnesium chloride, 3 mM manganese chloride, 0.003 mM sodium vanadate, 1.2 mM DTT, 50 g/mL PEG 20,000, 0.001 mM ATP, 1.5 ng/mL biotinylated polyGluTyr and 0.2  $\mu$ C  $^{33}$ P- $\gamma$ -ATP) and for EGFR (in 50 mM Tris, pH 8.0, 10 mM manganese chloride, 0.1 mM sodium vanadate, 1 mM DTT, 0.005 mM ATP, 1.5 ng/mL biotinylated polyGluTyr and 0.2  $\mu$ C  $^{33}$ P- $\gamma$ -ATP) in streptavidin coated FlashPlates (NEN, Boston, MA). Plates were sealed and read on the TopCount scintillation counter. Each measurement was performed at least in duplicate and the IC<sub>50</sub> values were calculated with standard deviation from two to eight separate experiments.
- A sandwich ELISA was developed utilizing two mouse monoclonal antibodies in a 96-well format. SK-BR-3 cells were treated for 24 h with serial dilutions of test compound or vehicle, and cell lysates were prepared. Lysates were transferred to a capture plate coated with a primary antibody-specific for the human extracellular domain of the ErbB-2 receptor. A horseradish peroxidase-conjugated anti-phosphotyrosine secondary antibody was used to detect the extent of phosphorylation of the immobilized ErbB-2 receptor. The chromogenic substrate, tetra-methylbenzidine (TMB) was used to measure the absorbance on a spectrophotometer at 450 nm.
- Antiproliferative activity of dual EGFR/ErbB-2 kinase inhibitors was assessed in monolayer cultures by  $^{14}$ C-thymidine incorporation into cellular DNA as described (Emanuel S. et al. *Mol. Pharm.* **2004**, *66*, 635) except that total time cells were exposed to drug was 96 h.
- Upstate Cell Signaling Solutions, Charlottesville, VA, USA.
- (a) PDB code is 2RGP. (b) EGFR cloning. The DNA sequence encoding amino acids S<sup>671</sup>–C<sup>998</sup> of human EGFR mature protein (Genbank Accession No. NM\_005228) was amplified by polymerase chain reaction (PCR) and inserted into the vector pDEST8 (Invitrogen) modified to include sequences encoding an in-frame hexameric histidine sequence and a thrombin cleavage site. The resulting construct thus encoded MHHHHHHVDLVPRGSHMA-(EGFR<sup>S671–C998</sup>) which was confirmed by DNA sequencing. This expression construct was then integrated into bacmid DNA and a recombinant isolate used to transfect SF9 insect cells as recommended by the vendor. The resulting baculovirus was then used to infect additional SF9 cells to increase viral titer and volume. (c) EGFR Purification. All purification processes were carried out on an ÄKTA FPLC system (GE Healthcare) at 4 °C. The purification protocol was performed as described previously [J. Biol. Chem. **2002**, *277*, 46265–46272]. Briefly, frozen cells were thawed and resuspended in 50 mM Tris, pH 7.5, 200 mM NaCl, 1% glycerol, 5 mM BME, 1 $\times$  complete EDTA-free protease inhibitor cocktail (Roche). Resuspended cells were dounce homogenized and mechanically lysed with an Emulsiflex-C5 (Avestin) at 10,000–15,000 psi. The lysate was clarified by centrifugation at 40,000g for 1 h. The supernatant was filtered through a 0.8- $\mu$ m vacuum filter and mixed to a TALON metal affinity resin (BD Biosciences) overnight at 4 °C. The lysate-TALON mixture was loaded into a column and washed with 10 column volumes of Buffer A (50 mM Tris, pH 8.0, 500 mM NaCl, 5 mM imidazole). EGFR was eluted using a 10-column volume linear gradient going from Buffer A to Buffer B (50 mM Tris, pH 8.0, 300 mM NaCl, 250 mM imidazole). Fractions containing EGFR, as assayed by SDS–PAGE, were pooled. Thrombin was added to the pooled protein to remove the histidine tag (0.005 U thrombin/ $\mu$ g EGFR). The reaction was dialyzed overnight against 50 mM Tris buffer, pH 8.0, 250 mM NaCl, 1 mM DTT. Cleaved EGFR was filtered through a 0.2- $\mu$ m SFC cartridge filter, concentrated, and loaded onto a Superdex 200 HR 10/30 column (GE Healthcare,) pre-equilibrated with 50 mM Tris, pH 8.0, 500 mM NaCl, 1 mM DTT. Fractions containing EGFR, as assayed by SDS–PAGE, were pooled and dialyzed against 10 mM Tris, pH 8.0, 1 mM DTT, 1 mM sodium azide, 0.1 mM benzamidine. (d) Crystallization, data collection, molecular replacement, and structure refinement of the EGFR-compound **17** complex. Purified human EGFR was concentrated to 4 mg/ml, complexed with compound **17** in a 1:2 ratio, and crystallized from a solution containing 2 M Na/K<sub>3</sub>PO<sub>4</sub>, 0.1 M Caps, pH 9.0, and 0.2 M Li<sub>2</sub>SO<sub>4</sub>.<sup>16</sup> X-ray diffraction data to a resolution of 2.0 Å were collected at the IMCA-CAT ID-17 beamline at the Argonne National Laboratory. Diffraction data were indexed, integrated, and scaled using the HKL2000 suite. The EGFR crystals belong to the P21212 space group, with unit cell parameters *a* = 45.85 Å, *b* = 68.03 Å, and *c* = 103.86 Å. The structure was determined by molecular replacement with CNX [Brunger, A. T.; Adams, P. D.; Clore, G. M.; DeLano, W. L.; Gros, P.; Grosse-Kunstleve, R. W.; Jiang, J. S.; Kuszewski, J.; Nilges, M.; Pannu, N. S.; Read, R. J.; Rice, L. M.; Simonson, T.; Warren, G. L. *Acta Crystallogr. D* **1998**, *54*, 905–921] using the structure of EGFR complexed with lapatinib as a search model (PDB ID 1XKK). All model building was done using O [Jones, T. A.; Zou, J. Y.; Cowan, S. W.; Kjeldgaard, M. *Acta Crystallogr. A* **1991**, *47*, 110–119], and refinement and map calculations were carried out using CNX [Brunger, A. T.; Adams, P. D.; Clore, G. M.; DeLano, W. L.; Gros, P.; Grosse-Kunstleve, R. W.; Jiang, J. S.; Kuszewski, J.; Nilges, M.; Pannu, N. S.; Read, R. J.; Rice, L. M.; Simonson, T.; Warren, G. L. *Acta Crystallogr. D* **1998**, *54*, 905–921]. The final structure was refined to an Rfactor of 22.7 and R<sub>free</sub> of 26.7.
- Wood, E. R.; Truesdale, A. T.; McDonald, O. B.; Yuan, D.; Hassell, A.; Dickerson, S. H.; Ellis, B.; Pennisi, C.; Horne, E.; Lackey, K.; Alligood, K. J.; Rusnak, D. W.; Gilmer, T. M.; Shewchuk, L. A. *Cancer Res.* **2004**, *64*, 6652. PDB ID 1XKK.